

# Observations of the $^{57}\text{Fe}^{+23}$ hyperfine transition in clusters of galaxies

H. Liang<sup>1,2,3</sup>, J.M. Dickey<sup>2,4</sup>, G. Moorey<sup>2</sup>, and R.D. Ekers<sup>2</sup>

<sup>1</sup> H.H. Wills Physics Laboratory, University of Bristol, Bristol BS8 1TL, UK

<sup>2</sup> Australia Telescope National Facilities, CSIRO, Epping, NSW 2112, Australia

<sup>3</sup> Institut d'Astrophysique Spatiale, Université Paris XI, F-91405 Orsay Cedex, France

<sup>4</sup> University of Minnesota, 116 Church St. SE, Minneapolis, MN 55455 USA

Received 3 March 1997 / Accepted 24 April 1997

**Abstract.** We present a search for the hyperfine transition of the  $^{57}\text{Fe}^{+23}$  ion at 3.071 mm in clusters of galaxies with the ATNF Mopra telescope. The results are compared with a realistic estimate of the peak brightness temperature of the line in a cooling flow cluster A85, using the available X-ray data.

**Key words:** galaxies: clusters – clusters of galaxies: individual Abell 85 – X-rays: galaxies – H II regions: 30 Dor

## 1. Introduction

It has been suggested by Sunyaev and Churazov (1984) that it might be possible to detect the hyperfine transition of a Li-like  $^{57}\text{Fe}^{+23}$  ion line in clusters of galaxies. Hyperfine transitions have been very important in astronomy. The first such transitions was predicted for neutral hydrogen atoms (the famous 21cm line) by van de Hulst in 1945 and detected in 1951. Atomic hyperfine splitting is the result of the interaction between the magnetic moment of the nucleus and the magnetic moment of the electron plus the magnetic field generated by the circulating electrons. In the case of the H I 21cm hyperfine transition at 1420 MHz, the ground state  $1^2S_{1/2}$  is split into 2 sublevels. Deuterium has a similar line predicted at 327 MHz but there have been no detections to date despite many efforts. The spontaneous transition probability (or Einstein coefficient) of the H I hyperfine transition is very low,  $W = 2.85 \times 10^{-15} \text{ sec}^{-1}$ . However, external excitation mechanisms such as collisions with other H atoms and electrons or  $\text{Ly}\alpha$  radiation increase the transition rates enormously. Hyperfine splitting is not present for all atoms or ions, since the interaction between the nuclear magnetic moment and the electronic magnetic moment does not occur if either of them is zero. We know from quantum mechanics that the total nuclear angular momentum (or nuclear spin) is zero for nuclei with an even number of protons and neutrons, and that the total

electronic angular momentum of an ion with completely filled electron shells is zero. Thus the commonly available isotope of iron  $^{56}\text{Fe}$  has no hyperfine structure. However, Sunyaev and Churazov (1984; SC) pointed out that the Li-like  $^{57}\text{Fe}^{+23}$  ion exhibits hyperfine structure with a higher spontaneous transition rate ( $W = 9.4 \times 10^{-10} \text{ sec}^{-1}$ ) than that of the H I hyperfine transition ( $W = 2.85 \times 10^{-15} \text{ sec}^{-1}$ ), which compensates the low abundance of the  $^{57}\text{Fe}$  isotope ( $^{57}\text{Fe}/^{56}\text{Fe}=2.3\%$ ; Vökening 1989). The wavelength of the  $^{57}\text{Fe}^{+23}$  hyperfine transition has been calculated theoretically to be 0.3071(3)cm (Shabaeva & Shabaev 1992). The FWHM of the line is 40 MHz (or 130  $\text{km s}^{-1}$ ), assuming a cluster gas temperature of  $2 \times 10^7 \text{ K}$  and that the line width is due to thermal Doppler broadening alone.

Clusters of galaxies are known to possess hot gas of temperature  $10^7 - 10^8 \text{ K}$ . This intracluster medium is found to be metal rich with typically half solar abundance (Sarazin 1988). The early X-ray observations detected the prominent “7 Kev Fe line” which is a blend of  $\text{Fe}^{+24}$  and  $\text{Fe}^{+25}$   $K\alpha$  and  $K\beta$  lines. The detection of this line not only provided the concrete proof that the primary X-ray emission mechanism for clusters is thermal bremsstrahlung, but also showed that the intracluster gas has nearly solar abundances and that at least some of the gas must have been ejected from galaxies. Other Fe lines at lower energy such as  $\text{Fe}^{+23}$  L lines have been detected at  $\sim 1 \text{ keV}$  in clusters. Thus we know that  $\text{Fe}^{+23}$  is abundant in cluster environments. SC had estimated the  $^{57}\text{Fe}^{+23}$  line strength in the centre of the Perseus cluster to be  $\sim 1.5 \text{ mK}$ , assuming a central temperature of 1.4 keV inside a 10-20 kpc radius with an X-ray emission integral of  $\sim 4.8 \times 10^{66} \text{ cm}^{-3}$ .

The detection of the  $^{57}\text{Fe}^{+23}$  line will have significant astrophysical implications on our understanding of the properties of the galaxy clusters. Firstly, it will provide us with a direct measure of the dynamics of the ICM, such as turbulence and accretion flows. There have been great debates on the formation of tailed radio sources in clusters of galaxies (e.g. Burns *et al.* 1986; O'Donoghue *et al.* 1993; Roettiger *et al.* 1993), with some suggesting that the sources are bent by their motions through the ICM and others suggesting that the bending is the

Send offprint requests to: H. Liang, [h.liang@bristol.ac.uk](mailto:h.liang@bristol.ac.uk)

result of an intracluster wind. This debate would benefit greatly from a direct measure of the intracluster turbulence. Secondly, mm observations of the  $^{57}\text{Fe}^{+23}$  line will complement the X-ray measurements of the distribution of iron in clusters and measure the  $^{57}\text{Fe}/^{56}\text{Fe}$  ratio which would determine the nucleosynthesis history of the intracluster gas. Finally, the mm line would provide a direct and high precision measure of the cluster redshift since the spectral resolution at mm-wavelength is much higher than in X-rays.

## 2. Observations

Our search for the  $\lambda$  3.1-mm  $^{57}\text{Fe}^{+23}$  line was carried out in 1996 September using the Mopra telescope of the Australia Telescope National Facility. The antenna is 22m in diameter of which the inner 15m is illuminated by the 3-mm feed, giving a beam width (FWHM) of  $45''$  and gain of  $40 \text{ Jy K}^{-1}$ . The receiver is a cooled SiS mixer with receiver temperature of 80 K which was checked with hot-cold load measurements twice during the seven day observation period. Pointing was tested by using SiO masers, the largest pointing error measured was  $10''$ . Atmospheric opacity was checked by skydips, the zenith opacity varied between 0.06 and 0.12 for all but a few hours during the run.

The spectrometer is an autocorrelator with two sections, each covering 256 MHz with 256 channels (1 MHz per channel). We overlapped these two by 125 MHz so as to cover a total bandwidth of 384 MHz. Roughly 50 MHz on each side are compromised by the IF filter shape, leaving a total bandwidth with consistent sensitivity of about 285 MHz which translates to  $920 \text{ km s}^{-1}$  at a wavelength of 3.2 mm (the redshifted wavelength). Since the line width is not well known, we do not remove baselines from the spectra, but simply edit the records on the basis of their raw rms noise.

Each record consists of a pair of two minute on and off source spectra from which we take the difference normalized by the bandpass shape. The reference position is offset by six minutes of right ascension. The expected spectral rms per record is about 20 mK, which is what we find in almost all cases. A few records ( $\sim 10\%$ ) show significantly higher noise due to baseline instabilities in the IF system. They are removed from the average. With this editing, the rms noise in the average decreases as integration time  $\sqrt{t_{int}}$  up to our maximum integration time of 10.5 hours. Because the spectra have not been baseline fitted, there remains some structure in the average spectra, but it is quite broad band (typically 100 MHz wide or greater). This baseline structure limits our ability to detect broad lines.

The clusters which we are searching for the  $^{57}\text{Fe}$  line are at redshifts of  $\simeq 0.06$ . Assuming rest frequency of  $97.611 \pm 0.03 \text{ GHz}$  ( $\lambda = 3.0713 \text{ mm}$ ) the cluster center frequencies come out in the range 92 - 92.5 GHz. More nearby clusters would not necessarily give stronger signals, since the beam size of  $45''$  translates to only  $35 \text{ h}^{-1} \text{ kpc}$  for a cluster at a redshift of  $16,000 \text{ km s}^{-1}$ . Thus the emission region is probably considerably larger than the beam. This is the reason for taking the reference position so far from the source.

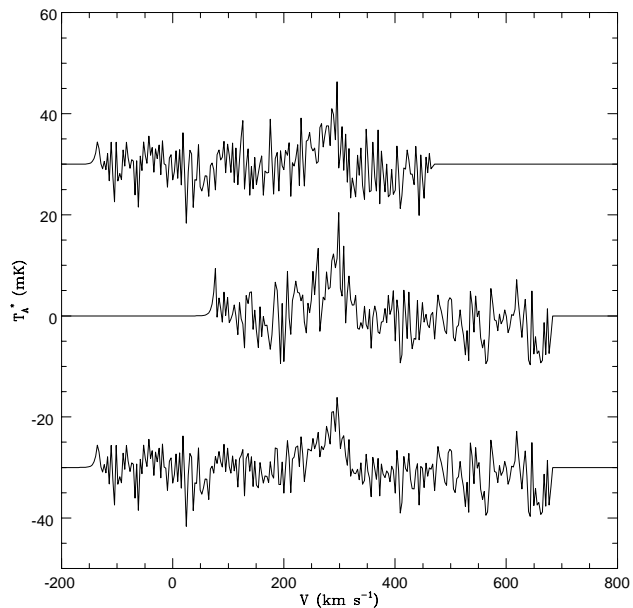


**Fig. 1.** Spectrum of the H41 $\alpha$  line from 30 Dor. The antenna temperature is plotted against the helio-centric velocity for the data from both spectrometer channels separately and combined. The vertical separations of 30 mK are for clarity in display and arbitrary.

As tests of the sensitivity and stability of our system and observing strategy, we have observed several calibration lines. The first test is simply to check the pointing using SiO masers at 86 GHz. We did these pointing checks every few hours for the first several days of the run observing five positions offset by a half beamwidth from the tabulated source position. We always detected the masers within  $10''$  of their nominal positions and with their nominal line strengths. Since both the beam size and the cluster sizes are much larger than this we have not introduced any pointing offsets. This test is limited in that the 86 GHz SiO frequency requires a different receiver tuning than the 92 GHz  $^{57}\text{Fe}$  line, so we checked the receiver performance by observing test lines at 92 GHz. The best candidates are  $^{13}\text{CS}$  line from Orion (SiO position) and M17SW, whose frequency is 92.494 GHz and the H41 $\alpha$  recombination line at 91.955 GHz which we observed in the 30 Dor region of the Large Magellanic Cloud. The  $^{13}\text{CS}$  line is so strong that it shows up in a single on-off pair, but the H41 $\alpha$  line is weak enough to provide a good test of a moderately long integration. Our spectrum of this test line is shown in Fig. 1; the position chosen was the 20-cm continuum peak at 05:38:46.675, -69:04:58.6 (J2000). The total integration time is 112 minutes and the noise level is 2.5 mK, 2.0 mK would be predicted by the radiometer equation, so the system is evidently performing well for integration times of an hour or so.

Table 1 lists the clusters which we have searched for  $^{57}\text{Fe}$  emission. Columns 1-3 give the cluster name and position, column 4 gives the integration time on-source, column 5 gives the detection threshold, and column 6 gives the useful velocity range. The detection threshold is a strong function of the width

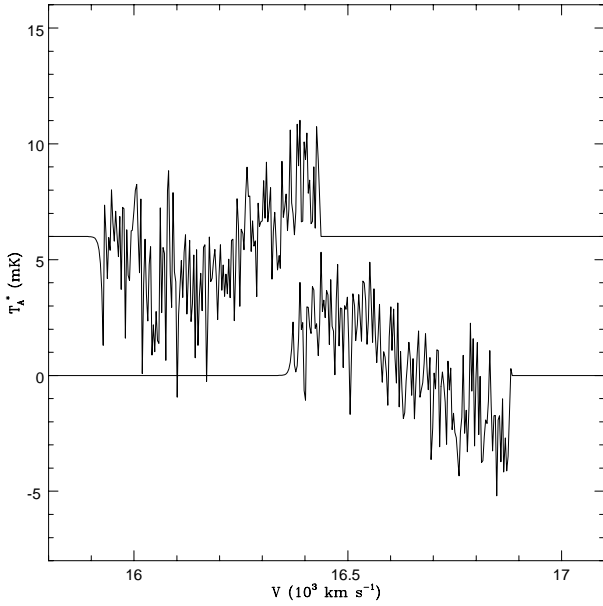


**Fig. 2.** Spectrum for the cluster A85. Antenna temperature is plotted against the helio-centric velocity for the 2 spectrometer channels separately. The vertical separation of 6 mK is arbitrary, for clarity in display.

**Table 1.** Summary of observations

Name	$\alpha$ (2000.0)	$\delta$ (2000.0)	$t_{int}$	$T_b$	$cz$ range
	h m s	° ' "	min.	mK	$10^2 \text{ km s}^{-1}$
A85	00 41 50.9	-09 18 10.7	630	5	160-168
A3266	04 30 33.4	-61 33 34.3	108	21	174-180
A3391	06 25 16.0	-53 39 39.0	124	20	160-168
A3667	20 12 27.4	-56 49 35.7	282	18	160-168

of the line because we have subtracted no baselines from our spectra. The threshold given on Table 1 applies to lines narrower than about  $150 \text{ km s}^{-1}$  in full-width. For broader lines the residual baselines in the receiver system begin to degrade our detection threshold. This effect is illustrated in Fig. 2, which is the pair of spectra for the cluster A85 for the two spectrometer channels. The vertical offset between the two is arbitrary, here it has been set at 6 mK for convenience. One channel is dominated by a linear baseline, while the other shows primarily a quadratic baseline shape. If we were to remove first and second order baselines and align the two channels we would obtain a spectrum with no features above 2 mK or less (depending on the smoothing). On the other hand, if cluster lines are as broad as several hundred  $\text{km s}^{-1}$  then this baseline removal could remove a real feature, and so our threshold would have to be raised; we cannot rule out the lump between 16200 and 16500  $\text{km/s}$  being part of a real feature of strength 3 mK and linewidth  $\simeq 300 \text{ km s}^{-1}$ . For linewidths of 200  $\text{km/s}$  or greater we must set the threshold at 5 mK in this case. For the other clusters on table 1 there are similar baseline irregularities that set the maximum linewidth corresponding to the threshold at about 150  $\text{km/s}$ .

### 3. Discussions and conclusion

Following the formalism given in Sunyaev and Churazov (SC;1984), we can calculate the expected line intensity for a cluster given the cluster gas parameters derived from X-ray observations.

The peak brightness temperature of the  $^{57}\text{Fe}^{+23}$  hyperfine transition should be

$$\Delta T_b = \frac{c^2}{8\pi^3/2\nu} \frac{h}{k} \frac{1}{\Delta\nu_D} \alpha \frac{g_u}{g_l} \Phi \quad (1)$$

where  $g_u, g_l$  are the statistical weights of the hyperfine sublevels,  $\Delta\nu_D$  is the Doppler line width (i.e. the half-width at  $e^{-1}$  of the maximum),  $\alpha$  is the cluster isotope abundance relative to hydrogen and the function  $\Phi$  is given by

$$\Phi = \int \frac{W\delta(T)\frac{1}{2}n_e^2\langle\sigma v\rangle}{W(1+N) + \frac{1}{2}n_e\langle\sigma v\rangle + \frac{g_u}{g_l}WN + \frac{g_u}{g_l}\frac{1}{2}n_e\langle\sigma v\rangle} dl \quad (2)$$

where  $W$  is the spontaneous transition probability,  $\delta(T)$  is the fraction of ions of a given species at temperature  $T$ ,  $N$  is the occupation number of the microwave background at the wavelength of transition,  $\langle\sigma v\rangle$  is the excitation coefficient by resonance scattering which is the dominant excitation process (SC). Note that Eq. (2) differs slightly from equation (2) in SC (see Appendix).

In the case of clusters of galaxies where  $WN \gg \frac{1}{2}n_e^2\langle\sigma v\rangle$  (or  $n_e \ll 1 \text{ cm}^{-3}$ ), Eq. (2) is reduced to

$$\Phi = \int \frac{\delta(T)\frac{1}{2}\langle\sigma v\rangle}{1+N + \frac{g_u}{g_l}N} n_e^2 dl \quad (3)$$

Assuming a constant temperature, we have from Eq. (1) and Eq. (3)

$$\Delta T_b \propto \int n_e^2 dl \propto S_x \quad (4)$$

where  $S_x$  is the X-ray surface brightness. If we assume solar abundance for clusters, where solar  $^{57}\text{Fe}$  abundance was taken to be  $8.8 \times 10^{-7}$  (SC), and isothermal cluster gas temperature within the Mopra beam to be at its optimum value of  $2 \times 10^7 \text{ K}$  where  $\delta(T)$  has its peak value of  $\sim 0.3$  (Jacobs *et al.* 1977), we can deduce a simple relation between the peak brightness temperature of the  $^{57}\text{Fe}$  line and the X-ray surface brightness:

$$\Delta T_b \sim 100 S_x \quad (5)$$

where  $\Delta T_b$  is the peak brightness temperature of the line in units of mK before convolution with the beam of the radio telescope, and  $S_x$  is the X-ray surface brightness in units of  $\text{ergs s}^{-1} \text{ cm}^{-2} \text{ ster}^{-1}$  in the ROSAT band of [0.1,2.4] keV after corrections for the telescope response and Galactic absorption. In the case of an average cluster of galaxies, where  $n_e \sim 10^{-3} - 10^{-2} \text{ cm}^{-3}$ , the peak brightness temperature would be  $\sim 0.001 \text{ mK}$ . However in the centre of cooling flow clusters of galaxies where the central density could be as high as

$n_e \sim 0.1 - 0.2 \text{ cm}^{-3}$ , the peak brightness temperature could only reach  $\sim 0.1 \text{ mK}$  in the most extreme cases, contrary to the estimate of  $\sim 1.5 \text{ mK}$  given by SC for the Perseus cluster.

The cluster A85 is considered a classic example of a cooling flow cluster with high X-ray luminosity and thus one of the best candidates for this experiment. To obtain a realistic prediction for the  $^{57}\text{Fe}$  line brightness for A85, we examine the X-ray data available for the cluster. The ROSAT PSPC data for A85 has been analysed by Pislár *et al.* (1996), who found an X-ray luminosity of  $9.3 \pm 0.2 \times 10^{44} \text{ ergs s}^{-1}$  within a radius of 1.4 Mpc in the ROSAT band of [0.1-2.4]keV. The X-ray surface brightness was fitted with a  $\beta$  model given by,

$$S_x \propto [1 + (r/r_c)^2]^{-3\beta+1/2} \quad (6)$$

which corresponds to

$$n_e(r) = n_0[1 + (r/r_c)^2]^{-3\beta/2} \quad (7)$$

for the electron density distribution, where  $n_0 = 0.01 \text{ cm}^{-3}$ ,  $\beta = 0.438$  and  $r_c = 32 \text{ kpc}$  ( $25''$ ). However, the surface brightness profile obtained with the ROSAT HRI (Prestwich *et al.* 1995) which has a resolution of  $5''$  (c.f.  $20''$  the PSPC) clearly shows that there is an excess above the  $\beta$  model within the central  $20''$  radius. Taking the X-ray surface brightness from HRI, we obtain from the above relation a peak brightness temperature of  $0.003 \text{ mK}$  for the  $^{57}\text{Fe}$  line. This predicted line brightness can be increased, if the abundance of  $^{57}\text{Fe}$  is significantly different from the terrestrial abundance and/or the distribution of Fe increases towards the centre. However, such effects are unlikely to increase the detectability of the line by more than a factor of 10.

This analysis shows that the expected brightness temperature of the  $^{57}\text{Fe}$  line to be  $\ll 1 \text{ mK}$  in cluster cores, even for an archetype cooling flow cluster such as Abell 85. We have shown that the MOPRA telescope can reach a sensitivity level comparable to the original prediction given by SC of the line intensity but is certainly inadequate given the more realistic estimates shown above.

*Acknowledgements.* We would like to thank Malcom Gray, Mike Masheder and Rashid Sunyaev for useful discussions, Graeme Carrad for helping with the instrument set up. HL would like to thank the ATNF and INSU (Franco-Australian collaboration fund) for support.

## Appendix A: derivation of Eqs. (1) and (2)

The number of transitions upwards equals to the number of transitions downwards:

$$n_u W + n_u B_{ul} B_\nu + n_u c_{ul} = n_l B_{lu} B_\nu + n_l c_{lu} \quad (A1)$$

where  $n_u, n_l$  are the number in the upper and lower states respectively,  $W$  and  $B$  are the Einstein A and B coefficients relating to spontaneous and stimulated emission/absorption,  $B_\nu$  is the intensity of the microwave background and  $c$  is the collisional

excitation/de-excitation rate. The  $W, B$  and  $c$  coefficients are related as follows (Rybicki and Lightman 1979):

$$B_{lu} = \frac{g_u}{g_l} B_{ul}, \quad B_{ul} B_\nu = W N, \quad c_{lu} = \frac{g_u}{g_l} c_{ul} \exp(-h\nu/kT) \quad (A2)$$

where  $N = (\exp(h\nu/kT) - 1)^{-1}$  is the occupation number of the microwave background. As was discussed in SC, the dominant excitation mechanism in this case is resonance scattering of an electron by the ion and the rate of excitation is given by  $c_{ul} = \frac{1}{2} n_e \langle \sigma v \rangle$ , where  $\langle \sigma v \rangle$  is the average of the product of the resonance scattering cross section and the relative velocity between the electron and the ion.

The peak intensity of the line is given by

$$I_0 = (N_u W + N_u B_{ul} B_\nu - N_l B_{lu} B_\nu) \frac{h\nu_0}{4\pi} \phi(\nu_0) \quad (A3)$$

where  $N_u, N_l$  are the total number of ions in the upper and lower levels per unit area along the line of sight respectively,  $W$  is the spontaneous emission coefficient or Einstein A-coefficient,  $\nu_0$  is the central frequency of the line and  $\phi$  is the line profile. Assuming thermal doppler broadening alone, we have

$$\phi(\nu) = \frac{1}{\sqrt{\pi} \Delta\nu_D} e^{-(\nu-\nu_0)^2/\Delta\nu_D^2} \quad (A4)$$

where  $\Delta\nu_D = \sqrt{\frac{2kT}{Mc^2}} \nu_0$  is the doppler width which is related to the FWHM  $\Delta\nu_L = 2\sqrt{\ln 2} \Delta\nu_D$ . In our case where  $h\nu \ll kT$ , we have the peak brightness temperature of the line given by  $\Delta T_b = \frac{c^2}{2k\nu^2} I_0(\nu_0)$ . By substituting Eq. (A1) into the expression for  $I_0$  in Eq. (A3), we have

$$\Delta T_b = \frac{c^2}{8\pi^{3/2}\nu} \frac{1}{\Delta\nu_D} \frac{h}{k} (N_l \frac{g_u}{g_l} \frac{1}{2} n_e \langle \sigma v \rangle - N_u \frac{1}{2} n_e \langle \sigma v \rangle) \quad (A5)$$

where

$$N_u = \int \alpha \delta(T) \frac{n_u}{n_l + n_u} \frac{n_H}{n_e} n_e dl \quad (A6)$$

with  $\frac{n_H}{n_e} \sim 1$  and  $\alpha \delta(T)$  giving the abundance of  $^{57}\text{Fe}^{+23}$  in the cluster, and  $N_l = (n_l/n_u) N_u$ . From Eq. (A1) and (A2), we have

$$\frac{n_u}{n_l} = \frac{g_u}{g_l} \frac{W N + \frac{1}{2} n_e \langle \sigma v \rangle}{W(N+1) + \frac{1}{2} n_e \langle \sigma v \rangle} \quad (A7)$$

Thus the peak brightness temperature is given by

$$\Delta T_b = \frac{c^2}{8\pi^{3/2}\nu} \frac{h}{k} \frac{1}{\Delta\nu_D} \alpha \frac{g_u}{g_l} \Phi \quad (A8)$$

where

$$\Phi = \int \frac{W \delta(T) \frac{1}{2} n_e^2 \langle \sigma v \rangle}{W(1+N) + \frac{1}{2} n_e \langle \sigma v \rangle + \frac{g_u}{g_l} W N + \frac{g_u}{g_l} \frac{1}{2} n_e \langle \sigma v \rangle} dl \quad (A9)$$

The term  $\frac{g_u}{g_l} \frac{1}{2} n_e \langle \sigma v \rangle$  in the denominator is absent in equation 2 of SC, however in cases where  $W N \gg \frac{1}{2} n_e^2 \langle \sigma v \rangle$  this term is insignificant.

## References

- Burns J.O., O'Dea C.P., Gregory S.A., Balonek T.J., 1986, ApJ 307, 73.
- Jacobs V.L., David J., Kepple P.C. & Blaha M., 1977, ApJ 211, 605.
- O'Donoghue A., Eilek J., Owen F., 1993, ApJ 408, 428
- Pislar V., Durret F., Gerbal D., Lima Neto G. B. & Slezak E., 1996, A&A in print.
- Prestwich A.H., Guimond S.J., Luginbuhl C.B. & Joy M., 1995, ApJ 438, L71.
- Roettiger K., Burns J.O., Loken C., 1993, ApJ 407, L53.
- Rybiki G.B. & Lightman A.P., 1979, *Radiative Processes in Astrophysics*, John Wiley & Sons.
- Sarazin C.L., 1988, in *X-ray Emission from Clusters of Galaxies*, Cambridge University Press
- Shabaeva M.B. & Shabaev V.M., 1992, Physics Letters A 165, 72.
- Syunyaev R.A. & Churazov E.M., 1984, Sov. Astron. Lett. 10(4), 201.
- Völkening J. & Papanastassiou D.A., 1989, ApJ 347, L43.